Available online at www.sciencedirect.com
SCIENCE DIRECT
Journal of Computational Physics 215 (2006) 465–484
JOURNAL OF COMPUTATIONAL PHYSICS
www.elsevier.com/locate/jcp

Kinetic energy conservation issues associated with the collocated mesh scheme for incompressible flow

Frédéric N. Felten *, Thomas S. Lund [1]

The University of Texas at Arlington, Department of Mechanical and Aerospace Engineering, Box 19018, Arlington, TX 76019-0018, United States

Received 30 June 2004; received in revised form 14 October 2005; accepted 7 November 2005
Available online 19 December 2005

Abstract

The collocated-mesh scheme is often favored over the staggered-mesh scheme for turbulence simulation in complex geometries due to its simpler form in curvilinear coordinates. The collocated mesh scheme does not conserve kinetic energy however, and few careful checks of the impact of these errors have been made. In this work, analysis is used to identify two sources of kinetic energy conservation error in the collocated-mesh scheme: (1) errors arising from the interpolations used to estimate the velocity on the cell faces, and (2) errors associated with the slightly inconsistent pressure field used to ensure mass conservation for the cell face volume fluxes. It is shown that the interpolation error can be eliminated through the use of first-order accurate centered interpolation operators with mesh-independent weights. The pressure error appears to be intrinsic to the scheme and it is shown to scale as $O(\Delta t^2 \Delta x^2)$. The effects of the conservation errors are investigated numerically through simulations of inviscid flow over an airfoil and in large eddy simulations of turbulent channel flow. Neither the interpolation error nor the pressure error appear to lead to significant problems in the channel flow simulations where viscous dissipation is present and where the Cartesian mesh is stretched in only one direction. The inviscid airfoil simulations performed on a curvilinear mesh show a much greater sensitivity to the interpolation error. The standard second-order centered interpolation is shown to lead to severe numerical oscillations, while the kinetic energy-conserving first-order centered interpolation produces solutions that are almost as smooth as those obtained with a third-order upwind interpolation. When compared in channel flow simulations, however, the first-order centered interpolation is shown to be far superior to the third-order upwind interpolation, the latter being adversely affected by numerical dissipation. Only slight differences were noted when comparing channel flow simulations using first-order and second-order centered interpolations. These results suggest that numerical oscillations can be controlled in curvilinear coordinates through the use of properly-constructed non-dissipative centered interpolations.

MSC: 65C30; 76F65

PACS: ; 47.11.+j; 47.27.Eq

* Corresponding author. Present address: GE Global Research Center, Fluid Mechanics Laboratory, One Research Circle, ES 500, Niskayuna, NY 12309, United States. Tel.: +817 296 0826.
E-mail addresses: felten@research.ge.com (F.N. Felten), tom.lund@colorado.edu (T.S. Lund).
[1] Present address: The University of Colorado at Boulder, Department of Aerospace Engineering Sciences, Boulder, CO 80309-0429, United States.

0021-9991/$ - see front matter © 2005 Elsevier Inc. All rights reserved.
doi:10.1016/j.jcp.2005.11.009

Keywords: LES; Conservation properties; Finite volume; Collocated grid; Curvilinear grid

1. Introduction

Numerical Simulation of turbulent flows, using either Direct Numerical Simulation (DNS) or Large Eddy Simulation (LES), requires high-fidelity numerical methods. For incompressible flow, it is highly desirable to have a scheme that conserves mass, momentum, and kinetic energy. In practice, it is rather difficult to satisfy these three constraints simultaneously and one is often faced with the need to give up strict conservation. For computations in Cartesian coordinates, solution methods for the incompressible Navier–Stokes equations have been successfully developed in the past using most often the staggered-mesh scheme since it is fully-conservative in this case. In recent years, more effort has been put in developing solution methods in curvilinear coordinates, however the extension of the staggered-mesh scheme to such coordinate system is not entirely straightforward leading many researchers to opt for simpler formulations. Foremost among these is the so-called collocated-mesh scheme, which has been used by a number of investigators [1,3,4,8,19,30,31], who were interested in performing turbulence simulations in complex geometries using body-fitted grids. It is important to notice that in this quest for simpler formulation in complex geometries, several other types of grid layouts have been studied with relative success for some of them [10,21,22].

Morinishi et al. [14] analyzed the conservation properties of several Finite-Difference (FD) schemes for both staggered- and collocated-grid arrangements. By restricting The analysis to Cartesian uniform meshes, Morinishi et al. showed that staggered-mesh methods can be made fully-conservative, whereas collocated-mesh methods will always contain an energy conservation error of the form $O(\Delta t^m \Delta x^n)$ due to the pressure formulation. Recently, Morinishi et al. [15] extended their work on non-uniform staggered grid, proposing a new finite difference scheme in cylindrical coordinates for incompressible flow. Their scheme conserves both momentum and kinetic energy for inviscid flow with the exception of the time marching error, provided that the discrete continuity equation is satisfied.

Although the FD and the Finite Volume (FV) approaches are equivalent on Cartesian uniform meshes [5], the FV approach seems to be more appropriate and thus widely spread in the Computational Fluid Dynamics community when problems involving curvilinear coordinates are solved. As a result, the FV approach has been adopted here to carry out the numerical solution of the Navier–Stokes equations and to perform the analysis of the conservation properties associated with the collocated-mesh scheme with boundary-fitted grid. The derivation shows that the collocated-mesh scheme may develop a second kinetic energy conservation error due to interpolation practices. The interpolation is necessary when information is needed at locations other than the center of the control volume. The popular second-order scheme, obtained by a straightforward linear interpolation between the two nodes on either side of the face, contains this extra source of kinetic energy conservation error, therefore creating the need to seek alternate interpolation operators.

Like the others before us, we were motivated to use the collocated-mesh scheme for complex flow LES due to it simpler form. Before doing this, however, we wanted to perform numerical experiments to investigate the impact of the kinetic energy conservation errors. We were also concerned with the prevalence of upwind interpolations used by prior investigators [4,8,19,30,31] when performing turbulence simulations with the collocated-mesh scheme in curvilinear coordinates, with more than one non-uniform direction and non-periodic boundary conditions. Any serious problems stemming from the kinetic energy conservation errors, or from the use of dissipative upwind interpolations would be grounds for us to reject the collocated-mesh scheme and simply code the staggered-mesh scheme in curvilinear coordinates [29].

In this study, three types of schemes are compared: (1) a properly-constructed (but first-order) central difference scheme where the advective terms are kinetic energy conserving on a general mesh, (2) an improperly-constructed (but second-order) central difference scheme that is not kinetic energy conserving on a general mesh, and (3) a third-order dissipative scheme. The third-order scheme is dissipative since the differencing stencil is not symmetric (i.e. upwind). One of the basic properties of FD schemes is that properly-constructed central schemes result only in phase error whereas upwind schemes always result in both phase and dissipation

errors [23]. This is true independent of the order of accuracy. While the third-order upwind scheme will always remove energy from the simulation by virtue of numerical dissipation, the improper second-order scheme may either *add or subtract* energy. Thus, while both the improper second order and the upwind schemes are non-conservative, the nature of the error can be rather different. The upwind scheme is expected to produce smooth solutions where the high-frequencies are damped by numerical dissipation. At the same time, one can be apprehensive about the improper second-order central scheme since its errors can act as energy sources which might lead to numerical instability. Finally, it can be anticipated that the proper first-order scheme should be stable and should not incorrectly damp the high frequencies. The fairly high magnitude of the phase errors, however, in the first-order scheme might be worrisome.

The objective of this work is twofold: (1) to clearly state the source of the conservation errors through analysis, and (2) to provide numerical results that address the suitability of the collocated-mesh scheme for turbulence simulation in generalized coordinates. The paper is organized as follows. The staggered-mesh and the collocated-mesh arrangements are presented in Section 2. The discrete operators used in this paper and the mathematical analysis of the kinetic energy conservation are derived in Section 3. Finally, the numerical results for the inviscid flow over an airfoil and for LES of turbulent channel flow are discussed in Section 4.

2. Grid arrangement

For numerical investigation of the incompressible Navier–Stokes equations with a structured computational grid, either the staggered-mesh arrangement or the collocated-mesh layout are often used depending on the level of complexity of the geometry.

2.1. Staggered-grid system

The staggered-mesh arrangement in curvilinear coordinates is shown in Fig. 1. The contravariant velocity components U_i (or U, V, W) are solution variables and are distributed around the pressure points p. This layout has the advantage that, when multiplied by the cell face area, the velocity components give the exact volume fluxes, F_i. This feature leads to a simplified mass balance computation and results in fully-coupled velocity and pressure fields.

When properly-formulated, the second-order staggered-mesh scheme should conserve mass, momentum, and kinetic energy, irrespective of the underlying coordinate system. In developing higher-order schemes, Morinishi et al. [14] first reviewed the conservation properties of several existing schemes cast in uniform Cartesian coordinates. They were able to show that all correctly-coded second-order accurate forms of the non-linear terms (divergence, advective, rotational, and skew-symmetric) are equivalent numerically and

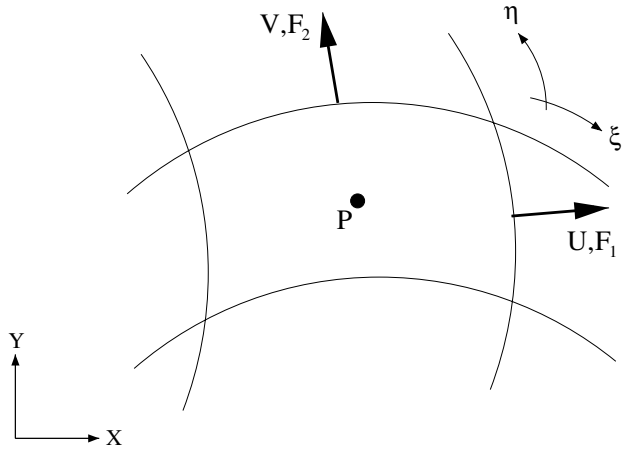

Fig. 1. Staggered-mesh arrangement in two-dimensional plane.

fully-conservative. Later Vasilyev [25] extended the work of Morinishi et al. to the case of non-uniform Cartesian meshes. In this work, Vasilyev advocated the use of a mapping to uniform computational space where grid-independent difference and averaging operators could be used. In spite of this, he chose to analyze the divergence form of the non-linear terms in physical space. He found that such a formulation does not conserve kinetic energy due to a lack of commutivity between the average and difference operators. This error can be dispensed with by choosing to work with the non-linear term written in the uniform computational space. The transformation is quite simple in the case of a non-uniform Cartesian mesh, and the fully-conservative formulation can be written as

$$\frac{\delta F_j}{\delta \xi_j} = 0, \tag{1}$$

$$\frac{\delta U_i}{\delta t} + \frac{1}{\overline{\mathscr{V}}^{\xi_i}} \frac{\delta}{\delta \xi_j} (\overline{U_i}^{\xi_j} \overline{F_j}^{\xi_i}) + \frac{\delta p}{\delta x_i} + (\text{visc})_i = 0, \tag{2}$$

where $\mathscr{V}$ is the cell volume, F_i is the volume flux, ξ_i is a computational space with unit displacements, and $(\text{visc})_i$ are the viscous terms. The commutation error discussed by Vasilyev [25] does not appear in this formulation since both the average and difference operations are performed in the uniform computational space. The only subtle point is that this formulation requires an average of the physical velocity components in the computational space (i.e. $\overline{U_i}^{\xi_j}$). Although this operation is easy to code (weights of 1/2), it results in a an approximation that is only first-order accurate. This same issue arises in the collocated mesh scheme and will be discussed in more detail in Section 3.

However, when using curvilinear coordinates, it is desirable to use the collocated arrangement which uses only one common control volume for all velocity component. As a result, it requires less memory storage and yields simpler equations than when the contravariant velocity components are employed [9,16,17,19].

2.2. Collocated grid system

The collocated-mesh arrangement in curvilinear coordinates is shown in Fig. 2. The Cartesian velocity components u_i (or u, v, w) are stored with the pressure, p, at the cell center. In addition, volume fluxes, F_i, are defined at the cell face in a manner analogous to the staggered-mesh system.

The volume fluxes are not solution variables, but rather are determined through interpolation of the cell-centered u_i values plus a projection operation that guarantees exact conservation of mass [18]. Use of the mass-conserving volume fluxes results in a pressure equation identical to that in the staggered-mesh system and thus also leads to fully-coupled velocity and pressure fields. While the pressure field determined in this manner leads to mass conserving volume fluxes, it leaves the primary solution variables, u_i, only approximately divergence

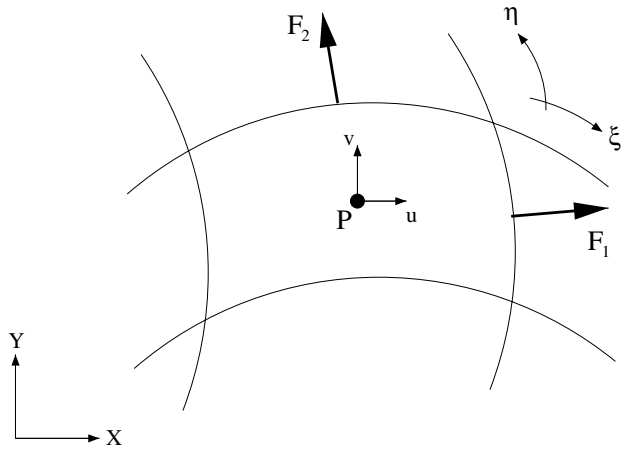

Fig. 2. Collocated-mesh arrangement in two-dimensional plane.

free. As pointed out by Morinishi et al. [14], and discussed in the next section, this defect leads to one source of kinetic energy conservation error.

3. Analysis

3.1. Finite volume approach

The mass and momentum conservation laws written in integral form are

$$\int_S (u_j n_j)\,\mathrm{d}S = 0 \tag{3}$$

$$\frac{\partial}{\partial t}\int_{\mathscr{V}} u_i\,\mathrm{d}\mathscr{V} + \int_S u_i(u_j n_j)\,\mathrm{d}S + \int_S p n_i\,\mathrm{d}S + (\mathrm{visc})_i = 0 \tag{4}$$

where u_i is the velocity described in Cartesian coordinates, p is the specific pressure (pressure divided by density), n_j is the outward-pointing normal vector and $(\mathrm{visc})_i$ represent a generic form of the viscous terms. The viscous terms will not be written out explicitly in what follows since we are concerned only with the kinetic energy conservation properties of the inviscid terms. The interested reader can find a clear description of the viscous terms in Ref. [5].

In the Finite Volume (FV) method, each computational cell makes up a control volume on which the integral conservation laws are enforced. A typical control volume (CV), together with the notation we shall use is shown in Fig. 3. For simplicity, we shall perform the analysis in two dimensions. Generalization to three dimensions is rather straightforward, does not require any extra assumptions and does not introduce any additional kinetic energy conservation issues as discussed in Section 4. The CV surface consists of four plane faces, denoted by lower-case letters (n, e, s, w) corresponding to their location with respect to the central node C. Adjacent nodes are denoted by upper case letters (i.e. N, NE, E, etc). Superscripts will be used throughout to denote the location where a quantity is evaluated. Subscripts i and j will always refer to Cartesian vector components. Thus, as shown in Fig. 3, the Cartesian components of the normal to the east face are denoted by n_j^{e}. Finally, displacements along the mesh lines connecting E–W points are denoted by the equivalent symbols ξ_{e} and ξ_{w}, whereas those corresponding to displacements along N–S points are denoted by ξ_{n} and ξ_{s}.

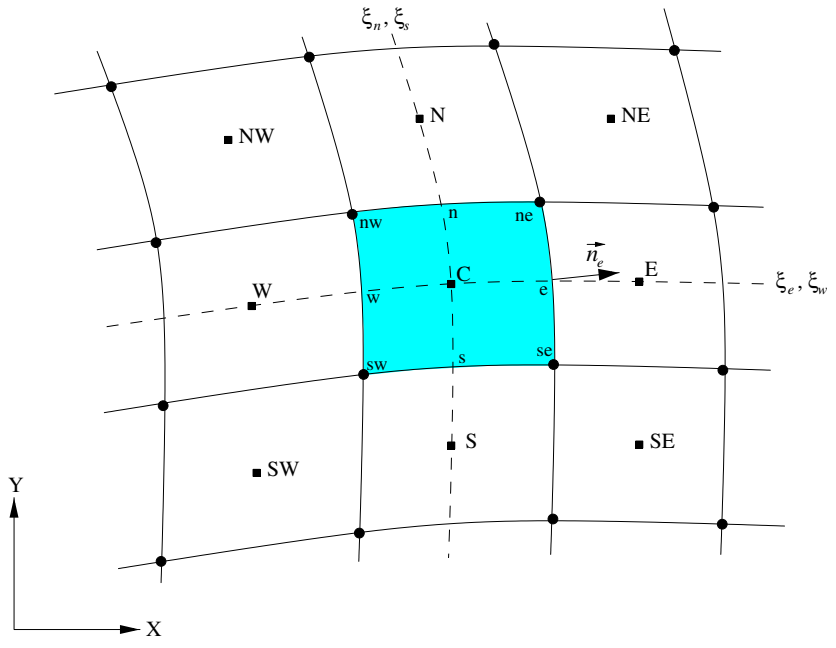

Fig. 3. A typical CV and the notation used for a 2D curvilinear grid.

The surface integrals in Eqs. (3) and (4) are approximated by the sum of the fluxes taken over the cell faces. Since the flow variables are stored at the cell centers, interpolation must be used to estimate the fluxes on the cell faces. The kinetic energy conservation properties of a given scheme are tightly linked to the details of the flux interpolation and we will pay great attention to this matter in what follows. For the moment, let $\overline{u_i}^l$ denote a generic interpolation of the velocity to the face $l \subset$ n, e, s, w. The details of the interpolation will be discussed in the following section.

For a second-order method, it is sufficient to treat both the interpolated velocity and the normal vector as constants over the extent of a cell face. Thus the surface integrals in Eqs. (3) and (4) can be approximated by simple products of the interpolated velocity and the face geometric properties. For example, an approximation to the mass conservation law takes the form

$$\int_S (u_j n_j)\,\mathrm{d}S \simeq \sum_{l=\mathrm{n,e,s,w}} \overline{u_j}^l \underbrace{n_j^l \Delta S^l}_{S_j^l} \tag{5}$$

where S_j^l is the surface area-weighted normal vector. Although this form of the mass conservation law is rather straightforward, it will result in pressure–velocity decoupling when the pressure projection is made. This situation is usually avoided by switching to a Rhie and Chow-type interpolation [18] for the cell mass flux F^l. For an incompressible method, this modification amounts to arranging the pressure Poisson equation so that the interpolated fluxes conserve mass exactly. This can be achieved in a fractional-step method by interpolating the intermediate velocity[2] to the face and then applying the pressure correction to these values. If the intermediate velocity is denoted by u_j^*, then the mass-conserving volume fluxes, F^l, are determined via

$$F^l = \overline{u_j^*}^l S_j^l - \alpha \Delta t \frac{S_j^l}{\mathscr{V}^l} \sum_{m(l)} p^m S_j^m \tag{6}$$

where α is a parameter associated with the time stepping method and $\mathscr{V}^l$ is the volume of the shifted cell centered around the midpoint of face l (see Fig. 4). The index m is used to denote the "face values" for the shifted cell. The index m consists of the collection of the nodal values C, N, E, S, and W, as well as the primary cell corner points ne, se, sw, and nw. As shown in Table 1, for each value of l, there is a unique set of four m values which correspond to the faces of the shifted volume centered around face l. Note that, although the pressure p^m is available directly when $m =$ C, N, E, S, W, interpolation must be used for the corner points (i.e. $m =$ ne, se, sw, nw). These latter interpolations must be bi-directional since the corner points are surrounded by four nodal values.

A Poisson equation for the pressure is generated by requiring that the volume fluxes in Eq. (6) sum to zero over each cell. This condition leads to

$$\sum_{l=\mathrm{n,e,s,w}} \sum_{m(l)} \left(\frac{S_j^l S_j^m}{\mathscr{V}^l} \right) p^m = \frac{1}{\alpha \Delta t} \sum_{l=\mathrm{n,e,s,w}} \overline{u_j^*}^l S_j^l \tag{7}$$

The only detail remaining in the discretization of the conservation laws is an approximation of the volume integral in Eq. (4). If the nodal point is located at the centroid of the cell, then a second-order approximation of the volume integral is simply the product of the nodal value, u_i, and the cell volume, $\mathscr{V}^{\mathrm{C}}$. Thus second-order finite-volume approximations to Eqs. (3) and (4) are

$$\sum_{l=\mathrm{n,e,s,w}} F^l = 0 \tag{8}$$

$$\mathscr{V}^{\mathrm{C}} \left(\frac{\delta u_i}{\delta t} \right) + \sum_{l=\mathrm{n,e,s,w}} \overline{u_i}^l F^l + \sum_{l=\mathrm{n,e,s,w}} \bar{p}^l S_i^l + (\mathrm{visc})_i = 0 \tag{9}$$

Note that the mass-conserving volume fluxes, F^l are also used in the momentum equation.

[2] The intermediate velocity arises from the first stage of the fractional-step method where a provisional time step is made using only advection and diffusion terms.

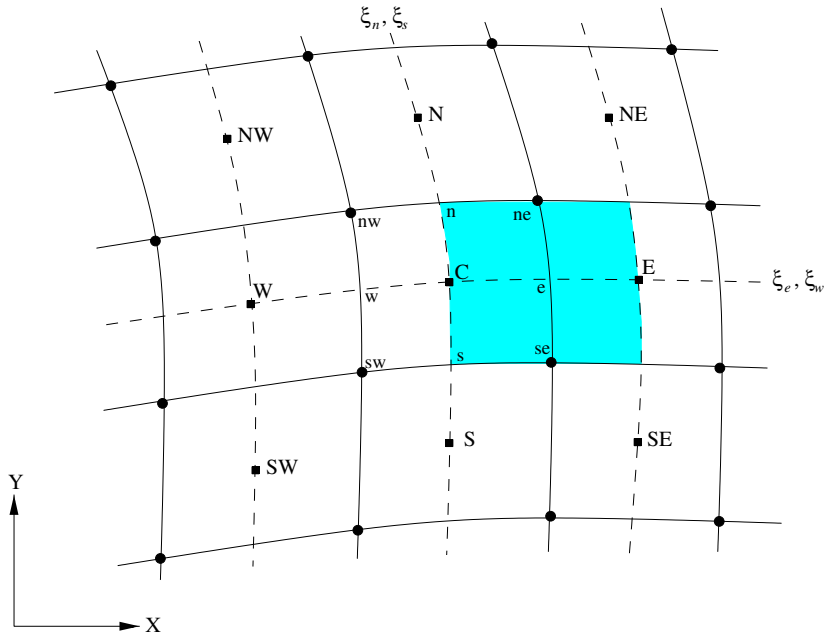

Fig. 4. Shifted volume used for the pressure correction. A volume centered around face 'e' is used for illustration. There are three other shifted volumes, one centered around each of faces n, s, and w.

Table 1
Correspondence between the face index l and the associated discrete points (index m)

l	$m(l)$
n	C, nw, N, ne
e	C, ne, E, se
s	C, se, S, sw
w	C, sw, W, nw

Since the pressure is determined to ensure that the face volume fluxes conserve mass, it is not possible to guarantee that the cell center values (u_i) remain solenoidal. However, the cell-center divergence can be kept to a minimum by employing the following pressure correction:

$$u_i = u_i^* - \frac{\alpha \Delta t}{\mathscr{V}^{\mathrm{C}}} \sum_{l=\mathrm{n,e,s,w}} \bar{p}^l S_i^l \tag{10}$$

The cell-center correction given above can be used to rewrite Eq. (6) as follows:

$$F^l = \overline{u}_j^l S_j^l - \alpha \Delta t \left[\frac{1}{\mathscr{V}^l} \sum_{m(l)} p^m S_j^m - \overline{\frac{1}{\mathscr{V}^{\mathrm{C}}} \sum_{q=\mathrm{n,e,s,w}} \bar{p}^q S_j^q}^{\,l} \right] S_j^l \tag{11}$$

The term in brackets above is proportional to the difference between two alternative approximations to the net pressure force. Each of these approximations are of order m, where $m = \min(2, n)$, and where n is the order of the interpolation. Since each term is of order m, the difference is also of order m. This result demonstrates that the Rhie and Chow interpolation [18] is an order m modification to the nodal velocity interpolated to the cell face. By summing the above relation over a cell and making use of Eq. (8), one can also infer that the cell-center divergence scales like $\Delta t \Delta \xi_l^m$. As discussed below, the Δt scaling for the flux interpolation and the cell-center divergence can be upgraded to Δt^2 through use of the Van Kan pressure correction scheme[24]. When this is done, the resulting $O(\Delta t^2 \Delta \xi_l^m)$ scaling implies that the cell-center divergence can be controlled to a fairly high degree.

3.2. Interpolation operators

With the idea of having to estimate fluxes on the faces of the CV, a wide variety of possibilities exist for the interpolations required by the finite volume scheme. In our framework, the approximations to the surface and volume integrals are restricted to second-order accurate schemes. It is easy to show that second-order accuracy can be achieved with a two-point stencil (i.e. by using only the two adjacent points). Using this approach, a general form for a quantity interpolated to the east face with a two-point stencil is

$$\bar{\phi}^{\mathrm{e}} \equiv (1-w)\phi^{\mathrm{C}} + w\phi^{\mathrm{E}} \tag{12}$$

where ϕ^{C} and ϕ^{E} are the adjacent nodal values (see Fig. 3), and where w is a weighting factor. This formula is second-order accurate if $w = |\Delta\xi_{\mathrm{eC}}|/|\Delta\xi_{\mathrm{E}}|$ and is first-order accurate otherwise. Here $\Delta\xi_{\mathrm{eC}}$ is the distance between the east face and the cell center, and $\Delta\xi_{\mathrm{E}} = \Delta\xi_{\mathrm{eC}} + \Delta\xi_{\mathrm{Ee}}$ is the approximate curvilinear distance between the central node and its neighbor to the east.

It is useful to rewrite the interpolation operator as the sum of two operators, one with the mesh-independent weights and a second containing the mesh information:

$$\bar{\phi}^{\mathrm{e}} = \underbrace{\frac{1}{2}[\phi^{\mathrm{C}} + \phi^{\mathrm{E}}]}_{\bar{\phi}^{\mathrm{e}_0}} + \underbrace{\left(w - \frac{1}{2}\right)\Delta\xi_{\mathrm{E}}}_{r_{\mathrm{e}}} \frac{\delta\phi}{\delta\xi_{\mathrm{e}}}, \tag{13}$$

where $\delta\phi/\delta\xi_{\mathrm{e}} = (\phi^{\mathrm{E}} - \phi^{\mathrm{C}})/\Delta\xi_{\mathrm{E}}$. In the next section we shall show that the second term above can be responsible for a kinetic energy conservation error.

For use in the kinetic energy conservation analysis, it is necessary to define a special interpolation operator for products. This operator was first introduced by Morinishi et al. [14]. Here it is simply restated using our notation. Again using the east face as an illustration, Morinishi's special interpolation operator for products takes the form

$$\widehat{\phi\psi}^{\mathrm{e}} = \frac{1}{2}(\phi^{\mathrm{C}}\psi^{\mathrm{E}} + \psi^{\mathrm{C}}\phi^{\mathrm{E}}) \tag{14}$$

These two interpolation operators given above can be generalized for interpolation to an arbitrary face l by writing

$$\bar{\phi}^{l} = \bar{\phi}^{l_0} + r_l \frac{\delta\phi}{\delta\xi_l}, \tag{15}$$

and

$$\widehat{\phi\psi}^{l} = \frac{1}{2}(\phi^{\mathrm{C}}\psi^{\mathrm{L}} + \psi^{\mathrm{C}}\phi^{\mathrm{L}}). \tag{16}$$

where C is the node of the primary cell and where L is the node of the adjacent cell displaced in the l direction. For example, if $l = \mathrm{e}$, then $L = \mathrm{E}$.

Morinishi et al. [14] also presented several identities involving combinations of interpolation and differentiation operators. One of these identities will be needed in the following section and thus it is restated here in finite-volume form. This relation is

$$\phi^{\mathrm{C}} \sum_{l=\mathrm{n,e,s,w}} \bar{\psi}^{l_0} Q^l + \psi^{\mathrm{C}} \sum_{l=\mathrm{n,e,s,w}} \bar{\phi}^{l_0} Q^l = \sum_{l=\mathrm{n,e,s,w}} \widehat{\phi\psi}^{l} Q^l + (\phi^{\mathrm{C}}\psi^{\mathrm{C}}) \sum_{l=\mathrm{n,e,s,w}} Q^l \tag{17}$$

where Q^l is a quantity known on the cell face (i.e. no interpolation needed). This relation can be specialized for our purposes by taking $\phi = u_i$, $\psi = p$, and $Q^l = S_i^l$. With these replacements, Eq. (17) can be rewritten as

$$u_i \sum_{l=\mathrm{n,e,s,w}} \bar{p}^{l_0} S_i^l = \sum_{l=\mathrm{n,e,s,w}} \widehat{u_i p}^{l} S_i^l + (u_i p^{\mathrm{C}}) \underbrace{\sum_{l=\mathrm{n,e,s,w}} S_i^l}_{=0} - p^{\mathrm{C}} \sum_{l=\mathrm{n,e,s,w}} \bar{u}_i^{l_0} S_i^l \tag{18}$$

Note that the second term on the right-hand side vanishes for a closed cell. A second variant of Eq. (17) is obtained by taking $\phi = u_i$, $\psi = u_i$, and $Q^l = F^l$. When this is done we obtain

$$u_i \sum_{l=\mathrm{n,e,s,w}} \overline{u_i}^{l_0} F^l = \sum_{l=\mathrm{n,e,s,w}} \left(\frac{1}{2}\widehat{u_i u_i}^{\,l}\right) F^l + \left(\frac{1}{2}u_i u_i\right) \underbrace{\sum_{l=\mathrm{n,e,s,w}} F^l}_{=0} \tag{19}$$

Again the second term on the right-hand side vanishes, this time due to the continuity relation (Eq. (8)).

3.3. Kinetic energy conservation

The kinetic energy equation is obtained by taking the dot product of the velocity with the momentum equation, and then using the continuity relation to simplify the result. The resulting equation can then be integrated over the domain to give the integral form of the kinetic energy equation. Continuous analysis shows that both the advective and pressure terms conserve kinetic energy since they can be written as flux integrals. Similarly, the discrete system will be conservative if the advective and pressure terms in the discrete kinetic energy equation can be put in flux form. In order to investigate this prospect, we multiply the discrete momentum equation by the velocity and then perform simplifications aimed at writing the product in flux form. It is convenient to treat the advective and pressure terms separately. Focusing first on the advective term, we rewrite the interpolation operation in Eq. (9) using Eq. (15), and multiply the result by u_i to get

$$u_i \sum_{l=\mathrm{n,e,s,w}} \overline{u_i}^{l} F^l = u_i \sum_{l=\mathrm{n,e,s,w}} \overline{u_i}^{l_0} F^l + u_i \sum_{l=\mathrm{n,e,s,w}} r_l \frac{\delta u_i}{\delta \xi_l} F^l \tag{20}$$

Now making use of Eq. (19), the above relation becomes

$$u_i \sum_{l=\mathrm{n,e,s,w}} \overline{u_i}^{l} F_l = \sum_{l=\mathrm{n,e,s,w}} \left(\frac{1}{2}\widehat{u_i u_i}^{\,l}\right) F^l + u_i \sum_{l=\mathrm{n,e,s,w}} r_l \frac{\delta u_i}{\delta \xi_l} F^l \tag{21}$$

The first term on the right-hand side is in flux form and is thus conservative. The second term can not be put in flux form and thus represents a kinetic energy error arising from the interpolation. Eq. (13) shows that this term is of order $(w - 1/2)\Delta\xi_{\mathrm{L}}$. Thus a small kinetic energy error exists unless $w = 1/2$. On a uniform mesh the $w = 1/2$ condition is satisfied and the advective terms are both second-order accurate and kinetic energy conserving. For non-uniform meshes there is a trade off between interpolation accuracy and kinetic energy conservation. If second-order interpolations are used on a non-uniform mesh, then $w \neq 1/2$ and the advective terms will not conserve kinetic energy. Alternatively, the advective terms can be constrained to conserve kinetic energy on a non-uniform mesh but the interpolation accuracy must be reduced to first order through use of mesh-independent weights of $w = 1/2$.

The kinetic energy conservation property of the pressure term is analyzed in a similar fashion. The interpolation operator defined in Eq. (15) is applied to the pressure term in Eq. (9) and the result multiplied by the velocity to get

$$u_i \sum_{l=\mathrm{n,e,s,w}} \bar{p}^{l} S_i^l = u_i \sum_{l=\mathrm{n,e,s,w}} \bar{p}^{l_0} S_i^l + u_i \sum_{l=\mathrm{n,e,s,w}} r_l \frac{\delta p}{\delta \xi_l} S_i^l \tag{22}$$

Now making use of Eq. (18), the above relation is rewritten as

$$u_i \sum_{l=\mathrm{n,e,s,w}} \bar{p}^{l} S_i^l = \sum_{l=\mathrm{n,e,s,w}} \widehat{u_i p}^{\,l} S_i^l - p \sum_{l=\mathrm{n,e,s,w}} \overline{u_i}^{l_0} S_i^l + u_i \sum_{l=\mathrm{n,e,s,w}} r_l \frac{\delta p}{\delta \xi_l} S_i^l \tag{23}$$

Finally, Eq. (11) is used to simplify the second term on the right-hand side. The final result is

$$u_i \sum_{l=\mathrm{n,e,s,w}} \bar{p}^{l} S_i^l = \sum_{l=\mathrm{n,e,s,w}} \widehat{u_i p}^{\,l} S_i^l - p \sum_{l=\mathrm{n,e,s,w}} F^l - p\alpha\Delta t \sum_{l=\mathrm{n,e,s,w}} \left[\frac{1}{\mathscr{V}^l} \sum_{m(l)} p^m S_i^m - \overline{\frac{1}{\mathscr{V}^{\mathrm{C}}} \sum_{q=\mathrm{n,e,s,w}} \bar{p}^q S_i^q}^{\,l_0}\right] S_i^l + u_i \sum_{l=\mathrm{n,e,s,w}} r_l \frac{\delta p}{\delta \xi_l} S_i^l \tag{24}$$

The first term on the right-hand side is in flux form and is thus conservative. The second term vanishes due to the continuity relation. The third term is a kinetic energy error arising from the fact that the cell-center

velocities do not conserve mass exactly. The final term is a kinetic energy conservation error due to the interpolation.

The advective and pressure error terms are added together to form $(\mathscr{E}_{\mathrm{ke}})_{\mathrm{coll}}$, the total error in kinetic energy conservation for the collocated-mesh scheme

$$(\mathscr{E}_{\mathrm{ke}})_{\mathrm{coll}} = \underbrace{u_i \sum_{l=\mathrm{n,e,s,w}} r_l \left(\frac{\delta u_i}{\delta \xi_l} F^l + \frac{\delta p}{\delta \xi_l} S_i^l \right)}_{\text{Interpolation Errors}} + \underbrace{p \alpha \Delta t \sum_{l=\mathrm{n,e,s,w}} \left[\overline{\frac{1}{\mathscr{V}^{\mathrm{C}}} \sum_{q=\mathrm{n,e,s,w}} \bar{p}^q S_i^q}^{l_0} - \frac{1}{\mathscr{V}^l} \sum_{m(l)} p_m S_i^m \right] S_i^l}_{\text{Pressure Error}} \tag{25}$$

This analysis shows that there are two sources of kinetic energy conservation error for the collocated-mesh scheme. The interpolation error will be present if second-order, mesh-dependent weighting factors are used. It can be eliminated by choosing first-order fixed weights of 1/2 ($r_l = 0$). Verstappen and Veldman [27,28] recognized the conservation error associated with mesh-dependent averaging weights and opted for constant weights of 1/2, in the case of a non-transformed staggered-mesh system.

Since the pressure error can not be eliminated, it is of interest to evaluate its scaling order. Let us focus on the term inside the square bracket in Eq. (25). To leading order, the $\overline{(.)}^l$ operator on the first term can be distributed. Furthermore, it is easy to see that $1/\overline{\mathscr{V}^{\mathrm{C}}}^l \simeq 1/\mathscr{V}^l$ and $\overline{S_i}^l \simeq S_i^m$. With this in mind, one can write

$$\overline{\frac{1}{\mathscr{V}^{\mathrm{C}}} \sum_{l=\mathrm{n,e,s,w}} S_i^l \bar{p}^l}^{l} - \frac{1}{\mathscr{V}^l} \sum_{m(l)} S_i^m p_m \simeq \frac{1}{\mathscr{V}^l} \sum_{m(l)} S_i^m \left(\overline{\bar{p}^l}^l - p_m \right) \simeq \frac{1}{\mathscr{V}^l} \sum_{m(l)} S_i^m \left(\Delta_{LC}^2 \frac{\delta^2 p_m}{\delta \xi_l^2} \right) \tag{26}$$

From the above equation, it is clear that the spatial pressure error scales like $\mathrm{O}(\Delta\xi^2)$. In addition, the $\mathrm{O}(\Delta t)$ dependence for the pressure error in Eq. (25) can be reduced to $\mathrm{O}(\Delta t^2)$ through the use of the Van Kan scheme [24]. In this formulation, one effectively projects with $\delta p = p^{n+1} - p^n \simeq (\partial p/\partial t)\Delta t$ instead of p in Eq. (11) and thus the terms proportional to p in Eq. (25) are reduced by a factor of Δt.

There are two important questions regarding the kinetic energy errors: (1) are the pressure errors strong enough to de-stabilize the scheme, and (2) does the kinetic energy violation due to second-order interpolations negate any increase in accuracy over the first-order (kinetic energy conserving) interpolations? These questions will be explored in the following section where the numerical experiments are presented and discussed.

4. Numerical results

4.1. Inviscid flow around an airfoil

The inviscid two-dimensional flow over a NACA-0012 airfoil at zero angle of attack has been considered to test the behavior of the collocated mesh arrangement in curvilinear coordinates. A C-mesh containing 400×128 grid-points with the outer boundary placed at three chords is used for the study. The external boundaries of the computational domain are presented in Fig. 5. The mesh is stretched in both the radial and azimuthal directions in order to better resolve the flow near the leading and trailing edges. For accuracy purposes the inflow boundary conditions are set using the values obtained from a potential flow solution, while a convective condition is implemented at the exit of the domain. A finite volume approach is used to treat the streamwise and wall-normal directions, while Fourier collocation is available in the spanwise direction for future computation in three dimension. The code makes use of a third-order Runge–Kutta explicit time marching scheme and the pressure Poisson equation is solved using a multigrid technique [2].

The simulation are performed using three different momentum interpolation operators: (1) the first-order centered interpolation, $w = 1/2$, only the second term in Eq. (25) is present, (2) the second-order centered interpolation, $w = \frac{|\xi_l - \xi_C|}{|\xi_L - \xi_C|}$, both terms in Eq. (25) are presents, and (3) the third-order upwind interpolation (QUICK-type [7]). We chose the third-order QUICK scheme due to its prevalence in earlier works. This is a well-constructed scheme that contains much lower dissipation levels than first or second-order upwind treatments.

In order to gain some insight into the conservative properties of the numerical schemes, we monitored the root mean square (rms) difference between the computed velocity field and the one obtained with a potential flow analysis. This rms quantity, $\mathrm{vel}_{\mathrm{rms}}$, is defined as

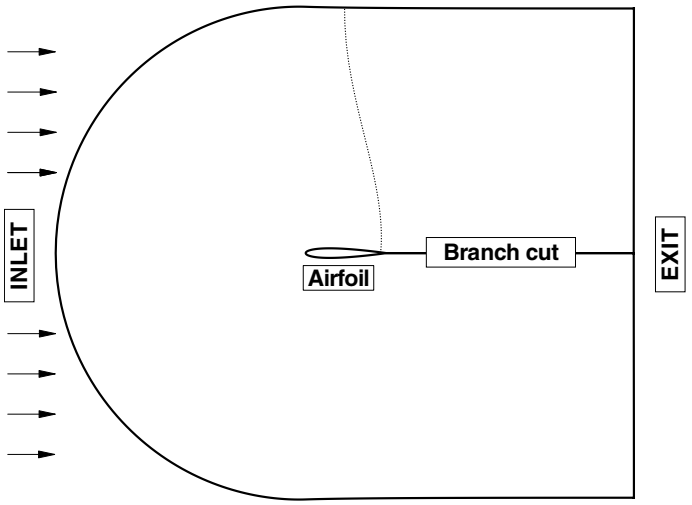

Fig. 5. Inviscid NACA-0012 airfoil flow: external boundaries of computational domain.

$$\mathrm{vel}_{\mathrm{rms}} = \sqrt{\frac{1}{N}\sum (u - u_{\mathrm{pf}})^2} + \sqrt{\frac{1}{N}\sum (v - v_{\mathrm{pf}})^2} \tag{27}$$

where u and u_{pf} are, respectively, the computed and the potential flow streamwise velocities; v and v_{pf} are, respectively, the computed and the potential flow wall-normal velocities, and N is the number of interior points in the computational domain. Fig. 6 shows the evolution of $\mathrm{vel}_{\mathrm{rms}}$, with respect to the dimensionless time $t^* = \frac{tU_\infty}{c}$, for the first-order centered interpolation and the second-order centered interpolation.

As expected for the first-order centered interpolation, $\mathrm{vel}_{\mathrm{rms}}$ remains constant while for the second-order interpolation it increases dramatically. Indeed lack of kinetic energy conservation for the second-order scheme is responsible for the oscillations. As discussed earlier, the energy conservation error in this case is of undetermined sign and thus it acts as both sources and sinks. The sources produce high-frequency oscillations that grow with time through a feedback mechanism (see Fig. 6). The following post-processing of both the pressure field and the velocity field at a dimensionless time $t^* \simeq 7.8$, will corroborate this claim, indicating that the solution obtained with the second-order centered interpolation is getting further and further away from a solution obtained by potential flow analysis.

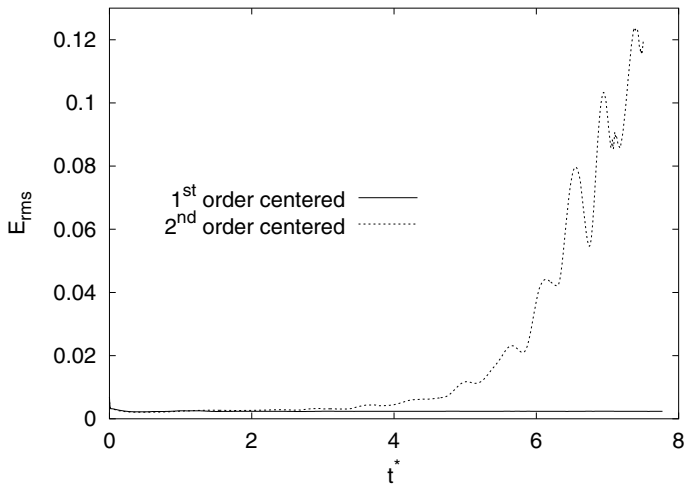

Fig. 6. Inviscid NACA-0012 airfoil flow: time evolution of $\mathrm{vel}_{\mathrm{rms}}$.

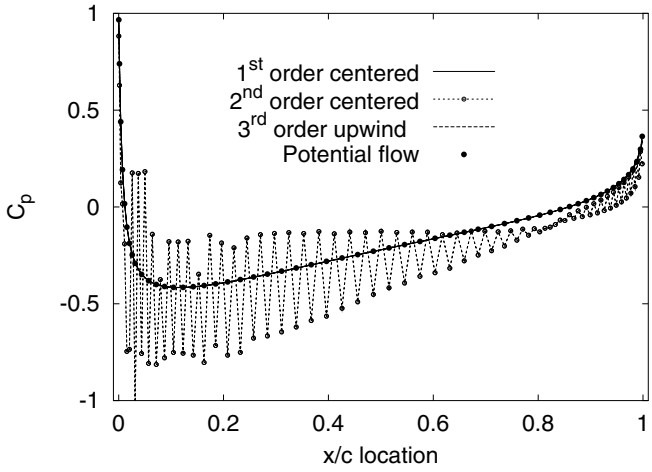

Fig. 7. Inviscid NACA-0012 airfoil flow: pressure coefficient distribution.

Fig. 7 shows the distribution of the pressure coefficient along the airfoil for the three operators considered. The results for the first-order centered and third-order upwind interpolations are in good agreement with the results of a potential flow analysis. The results for the second-order centered interpolation, on the other hand, show very strong oscillations. More insight can be gained from a comparison of the streamwise velocity contours shown in Fig. 8. As expected, the dissipative third-order upwind interpolation gives the smoothest solution. It has an error term that is purely dissipative resulting in a smooth solution where the low-frequency solution components are computed accurately. The associated non-physical attenuation of high-frequency solution components has virtually no ill effect in this case since the mean flow solution is very well described by the low-frequency components. This is the reason why upwind schemes are so popular. They are ideal for most conventional CFD calculations (including Reynolds averaged turbulent cases) where only the mean flow solution is sought. The first-order centered interpolation gives a reasonably smooth solution that is comparable to the upwind interpolation, while on the opposite extreme, the second-order centered interpolation produces a flow field that is obscured by numerical oscillations. Thus it is quite fair to say that the kinetic energy conservation is not a critical issue for mean flow calculations, unless it is of undetermined sign and results in numerical instability.

Our first-order kinetic energy conserving scheme is at a disadvantage for the airfoil calculation since it strives to retain small-scale energy. This feature results in some small amplitude point-to-point oscillations. These residual oscillations are noticeable for the first-order interpolation in the region near the trailing edge of the airfoil (see Fig. 8). A commonly used trick for improving the visual quality of solutions with oscillations arising from energy conserving schemes is to plot the solution averaged to the cell face. This operation eliminates the point-to-point oscillations and is consistent with either the first or second-order approximations. Had we done this, the first-order solution would have appeared to be nearly identical to the third-order upwind solution. We chose not to do this, however, since we wanted to present our scheme as honestly as possible.

With this in mind, the intensity of these oscillations is investigated using the quantity I_{osc}, defined as

$$I_{\text{osc}} = \left|\frac{u_{\text{pf}} - u}{u_{\text{pf}}}\right| = \left|1 - \frac{u}{u_{\text{pf}}}\right| \tag{28}$$

The maximum intensity of the oscillations for that particular region of the field is extremely small, $I_{\text{osc}}^{\max} \simeq 0.1\%$. To emphasize the above claim, Figs. 9 and 10 show the streamwise velocities, for the first-order centered interpolation and the potential flow solution, plotted along the dotted line shown in Fig. 5. The residual oscillations are undetectable in Fig. 9. Fig. 10 shows that it is only after restricting the ordinate between 0.95 and 1.01, for the streamwise velocities, that the presence of some minor oscillations is revealed.

It is concluded that, even though some residual oscillations are present in the field with the use of the first-order centered interpolation; they are extremely weak, do not grow out of bound with time and do not seem to

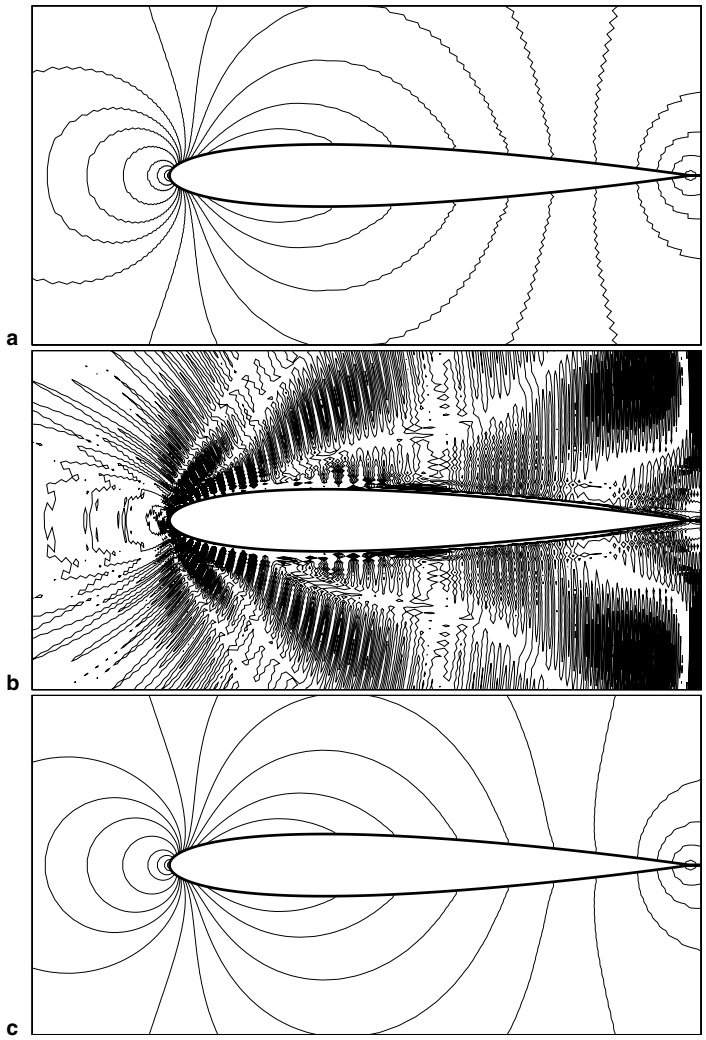

Fig. 8. Inviscid NACA 0012 airfoil flow: streamwise velocity contours. (a) First-order centered interpolation, (b) second-order centered interpolation, and (c) third-order upwind interpolation.

affect the solution. These results are rather significant since they imply that numerical oscillations can be controlled without resort to dissipative upwind schemes. As we will show in the next section, the numerical requirements for mean flow calculations and for turbulence simulation are rather different. While dissipative schemes are ideal for mean flow calculations, they are not well suited for large eddy simulation where the effects of dissipation have a large negative impact on the solution.

4.2. Turbulent channel flow

The influence of the two sources of kinetic energy conservation error are evaluated through LES of plane channel flow at $Re_\tau = 400$, based on the channel half width and friction velocity. Two computer codes are used; one is based on the staggered-mesh arrangement in the form of Eq. (2) and the other is based on the collocated-mesh arrangement. In either case, finite differences are used only in the streamwise and wall-normal directions and Fourier collocation is used in the spanwise direction. This arrangement allows for more efficient convergence studies since it is only necessary to vary the mesh spacings in the x and y directions in order to investigate the effects of the numerical error. Both codes make use of a third-order Runge–Kutta explicit time marching scheme. The spanwise direction is de-aliased at no computational expense through the use of mesh

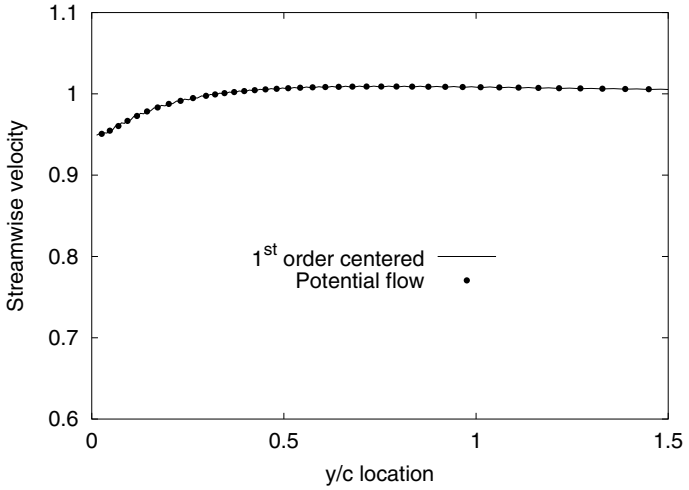

Fig. 9. Inviscid NACA 0012 airfoil flow: streamwise velocity along dotted line of Fig. 5.

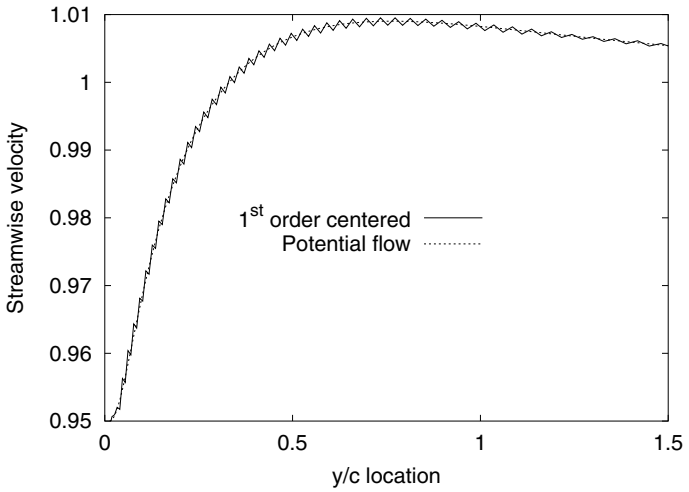

Fig. 10. Inviscid NACA 0012 airfoil flow: minor oscillations of the streamwise velocity.

shifting [20]. This is done in concert with the multi-step Runge–Kutta scheme. The pressure Poisson equation is solved directly via Fourier transforms in x and z and tri-diagonal inversion in y direction.

4.2.1. Influence of the pressure error

In order to exclusively study the influence of the pressure error when the collocated-mesh arrangement is used, the two codes were run using a first-order centered interpolation. The staggered-mesh arrangement is then fully-conservative, while only the pressure error is present for the collocated layout.

Three mesh resolutions and several time step sizes are investigated in order to study the effect of the discretization and the time stepping errors (see Table 2). The computational domain is $8\delta \times 2\delta \times 2\delta$, where δ is the channel half width. The subgrid-scale stresses are modeled using the dynamic model [6]. The results are compared with the DNS data of Moser et al. [12] for $Re_\tau = 395$. It is generally believed that the low-order statistics computed via LES should converge to the true solution (i.e. DNS) as the mesh is refined. This will happen as long as the energy peak and inertial range portions of the spectrum resolved in the LES agree with the DNS. For the convergence studies, the time step was held fixed for the three mesh resolutions. This time step corresponds to the viscous stability limit on mesh C.

Table 2
Mesh spacings used for the LES of turbulent plane channel flow

Case	N_x	N_y	N_z	Δx^+	Δy^+	Δz^+	$\Delta t \cdot u_\tau/\delta$
A	16	16	32	200	4–127.15	25	9.1×10^{-4}
B	32	32	32	100	2–62.63	25	9.1×10^{-4}
C	64	64	32	50	1–30.91	25	9.1×10^{-4}

Fig. 11 shows the mean velocity profiles for the three mesh resolutions. As expected, both the staggered and collocated results improve as the resolution is increased. The staggered-mesh results are consistently closer to the DNS data for the two coarsest grid, and a very good agreement is achieved in the sublayer and log region on the finest mesh (case C) for both mesh arrangements. Since the collocated mesh scheme in conjunction with the Van Kan scheme [24] has a kinetic energy conservation error that scales like Δt^2, we investigated the possibility that the differences in Fig. 11 are from this source. The time step was reduced by 50% on mesh C, and increased by 400% on mesh B. In either case, the results were almost invariant to changes in the time step.

Fig. 12 shows a comparison of the turbulent velocity fluctuations. For the sake of clarity, only results for u_{rms} and v_{rms}, for cases A and C are shown. Once again the staggered-mesh results are superior to the

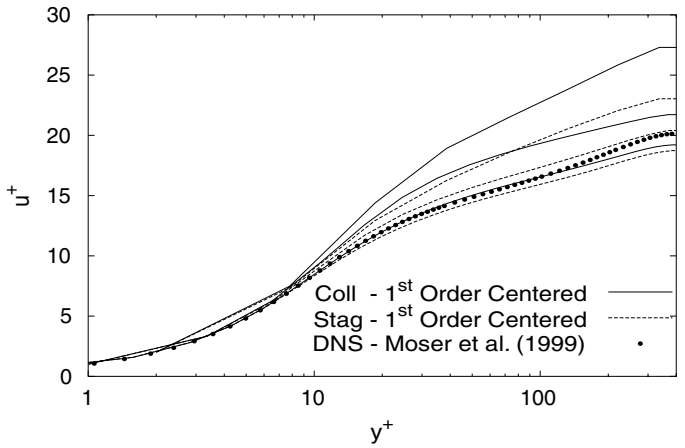

Fig. 11. Convergence of the mean velocity profile.

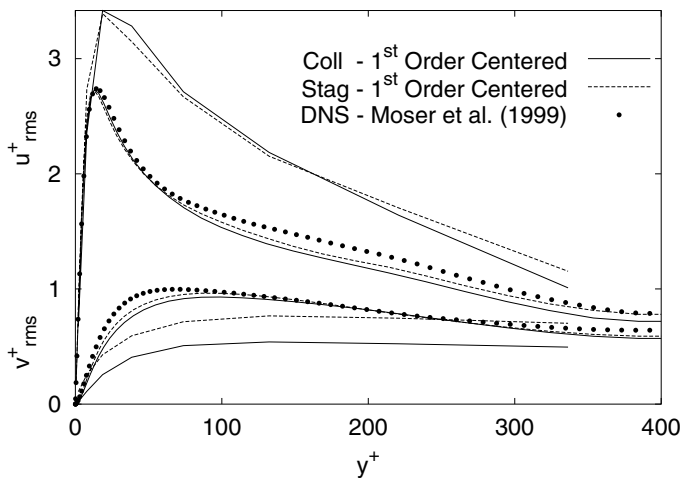

Fig. 12. Convergence of the velocity fluctuations.

collocated-mesh at all resolutions. The DNS data were not filtered and thus some of the apparent difference between the LES and DNS is due to the unresolved energy in the LES. This effect should be minimal on mesh C. The differences between the two schemes on the finest mesh (C) are minor and either method produces reasonable results at this resolution. The velocity fluctuation profiles are also rather insensitive to changes in the time step.

In conclusion, it is fair to believe that the pressure errors in the collocated mesh scheme do not have a visible impact on the results, provided that the simulation are run at a sufficiently high mesh resolution.

4.2.2. Influence of the interpolation operator

In order to check the influence of the momentum interpolation operator for turbulent flow simulation, we used, similarly to the inviscid NACA-0012 airfoil case, a first-order centered interpolation, a second-order centered interpolation, and a third-order upwind interpolation.

First, in an effort to be thorough, the convergence of the third-order upwind scheme is investigated. Plots comparable to the one displayed in Figs. 11 and 12 are presented, respectively, in Figs. 13 and 14 for the QUICK scheme. Analogously to the first and second-order centered schemes, the results improve as the mesh

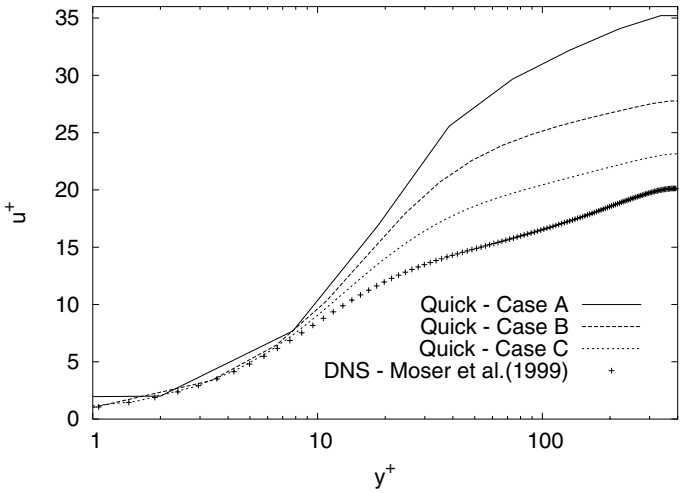

Fig. 13. Third-order upwind—convergence of the mean velocity profile.

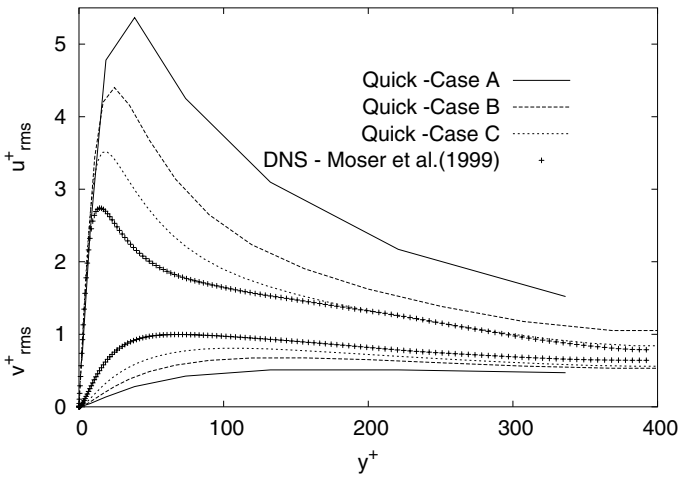

Fig. 14. Third-order upwind—convergence of the velocity fluctuations.

resolution increases but with much larger errors since the high frequency portion of the energy spectrum is eroded due to numerical dissipation.

Figs. 15 and 16 show respectively, the mean velocity profiles and the turbulent velocity fluctuations, obtained on mesh C, for the three momentum interpolation. Note that for the sake of clarity only results for u_{rms} and v_{rms} are plotted in Fig. 16.

Both the first-order centered and the second-order centered interpolation agree relatively well with the DNS data, with the first-order centered interpolation holding superior results. As expected from previous studied performed by Mittal and Moin [13], the use of third-order upwind interpolation degrades the results considerably.

After ruling out the use of up-winding interpolation, it is of interest to focus on the effect of locally lowering the order of accuracy from second to first order, when using the first-order centered interpolation. The rate of convergence of the LES results to the DNS data was then investigated, for the first-order and the second-order interpolation, by forming the rms difference between the LES and DNS mean velocity profiles:

$$E_{\mathrm{rms}} = \sqrt{\frac{1}{2\delta}\int_0^{2\delta} (u_{\mathrm{LES}} - u_{\mathrm{DNS}})^2 \,\mathrm{d}y} \tag{29}$$

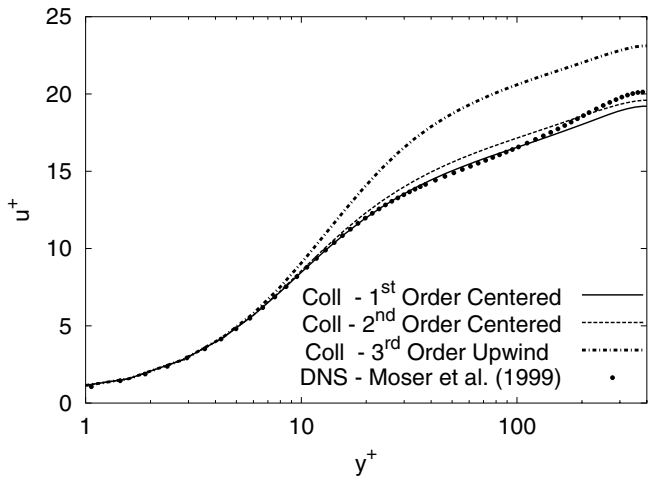

Fig. 15. Mean velocity profile for specific interpolation operator.

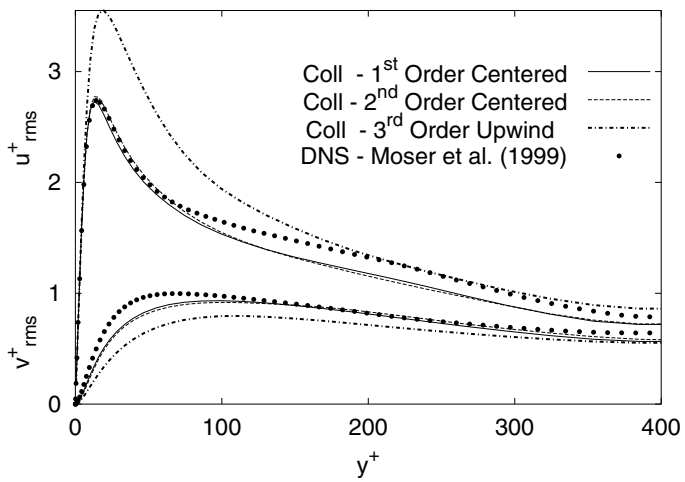

Fig. 16. Velocity fluctuations for specific interpolation operator.

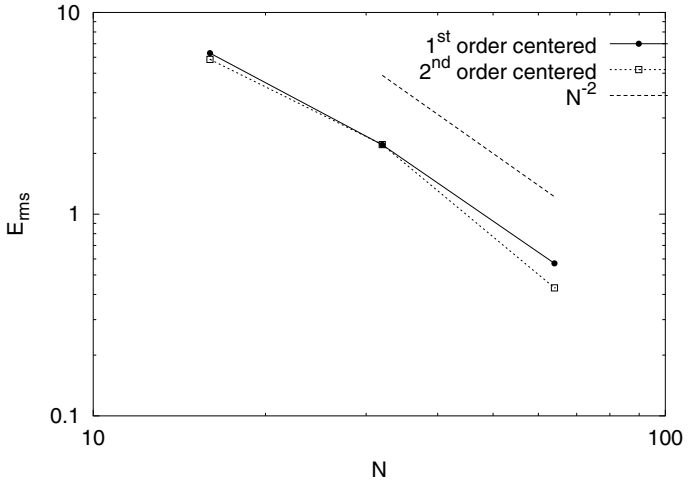

Fig. 17. Convergence history as a function of the mesh resolution.

Fig. 17 shows the E_{rms} for both momentum interpolation as a function of the grid resolution. The two operators behave similarly and the second-order interpolation appears to converge at a slightly higher rate. The second-order interpolation solution has a slightly smaller rms error as compared with the first-order interpolation solution, on mesh C, even though Fig. 15 would suggest the opposite. The reason for this is that Fig. 15 is plotted on a log scale, which emphasizes the near-wall region. Even though the local truncation error is first order for the first-order momentum interpolations, the global discretization error shows a convergence rate close to second order between the finest two meshes. This interesting feature, previously discussed by Veldman and Rinzema [26], was brought out by Manteuffel and White [11]. They proved that the global discretization error, for slowly varying grids with appropriate boundary condition, is of second order if the change in mesh size is restricted such that $\Delta_{i+1} - \Delta_i = \mathrm{O}(\Delta^2)$, where $\Delta = \max(\Delta_i)$. Since the mesh, used for the LES of plane channel, is stretched respecting the above criterion in the wall-normal direction, the second-order convergence rate between the finest two meshes is expected.

5. Conclusions

We have shown that, in general, the collocated-mesh scheme, often chosen over the classical staggered-mesh arrangement in curvilinear coordinates, violates kinetic energy conservation due to two sources: (1) pressure errors and (2) interpolation errors.

It does not appear possible to eliminate the first source of kinetic energy conservation error (pressure error). It is possible, however, to limit the size of this error to $\mathrm{O}(\Delta t^2 \Delta x^2)$. We could not discern any evidence of this error in turbulent channel flow simulations, where its magnitude was varied by a factor of 16 through time step refinement. These results suggest that pressure term is probably not a serious issue for LES where reasonably fine meshes and small time steps are required for general accuracy purposes.

The second of these sources can be eliminated through the use of mesh-independent centered interpolation operators. Although these operators are formally only first-order accurate, they are multiplied by geometric terms that are of the order of the mesh spacing for practical computations. We observed second-order convergence under mesh refinement for typical LES meshes used in turbulent channel flow. The kinetic energy conservation errors associated with second-order centered interpolations were shown to lead to fairly severe numerical oscillations in a test case involving the inviscid flow around an airfoil computed in curvilinear coordinates. The oscillations could be controlled either by switching to a kinetic energy-conserving first-order centered interpolation, or by switching to a third-order upwind interpolation. Since the use of dissipative interpolation for turbulent simulation strongly degrades the results, we favor the centered interpolation approach.

A curious feature with our tests is that there is no correlation between the order of accuracy and the nature of the numerical error. While the magnitude of the numerical error certainly decreases with the order of accu-

racy, the effect of the numerical error on turbulence actually increases. From earlier work [13], we know that large eddy simulation of turbulence requires that the smallest resolved scales retain the correct energy level. Dissipative schemes are very effective at eroding small scale energy proving the simulation results to suffer noticeably. Numerical dissipation, even at high order, is more detrimental to large eddy simulation than is pure phase error at lower order. While this may seem counter-intuitive, the numerical error in conservative schemes appears to the turbulence as a high-frequency phase scrambling term. Previous researchers [13] have shown clearly that, while turbulence is very sensitive to artificial attenuation of small-scale energy, it is surprisingly indifferent to phase scrambling.

Overall, this work suggests that the use of dissipative upwind interpolations may be unnecessary when the collocated-mesh scheme is applied in complex body-fitted geometries. This would significantly increase the fidelity of the numerical method for LES applications.

Acknowledgements

Bell Helicopter Textron Inc. and the National Rotorcraft Technology Center are gratefully acknowledged for financially supporting this research. The authors would like to thank Dr. R.W.C.P. Verstappen for his comments and Dr. R. Mittal for his helpful suggestions regarding the multigrid solver.

References

[1] V. Armenio, U. Piomelli, A Lagrangian mixed subgrid-scale model in generalized coordinates, Flow Turbul. Combust. 65 (2000) 51.
[2] A. Brandt, Multilevel adaptive solutions to boundary value problems, Math. Comput. 31 (1977) 333.
[3] N. Chidambaram, R.H. Pletcher, A collocated-grid, fully coupled algorithm for large eddy simulation of incompressible and compressible flows, Numer. Heat Transfer Part B 37 (2000) 1.
[4] G.S. Constantinescu, K.D. Squires, LES and DNS investigations of turbulent flow over a sphere, AIAA Paper 2000-0540, 2000.
[5] J.H. Ferziger, M. Peric, Computational Methods for Fluid Dynamics, Springer-Verlag, New York/Berlin, 1996.
[6] M. Germano, U. Piomelli, P. Moin, W.H. Cabot, A dynamic subgrid-scale eddy viscosity model, Phys. Fluids A 3 (1991) 1760.
[7] B.P. Leonard, A stable and accurate convection modeling procedure based on quadratic upstream interpolation, Comput. Methods Appl. Mech. Engrg. 19 (1979) 59.
[8] F.S. Lien, M.A. Leschziner, A general non-orthogonal collocated finite volume algorithm for turbulent flow at all speeds incorporating second-moment turbulence-transport closure, Part 1: Computational implementation, Comput. Methods Appl. Mech. Engrg. 114 (1994) 123.
[9] M. Majumdar, Role of underrelaxation in momentum interpolation for calculation of flow with non-staggered grids, Numer. Heat Transfer 13 (1988) 125.
[10] C.R. Maliska, G.D. Raithby, A method for computing three dimensional flows using non-orthogonal boundary-fitted coordinates, Int. J. Numer. Methods Fluids 4 (1984) 519.
[11] T.A. Manteuffel, A.B. White Jr., The numerical solution of second-order boundary value problems on nonuniform meshes, Math. Comput. 47 (1986) 511.
[12] R.D. Moser, J. Kim, N.N. Mansour, Direct numerical simulation of turbulent channel flow up to $Re_\tau = 590$, Phys. Fluids 11 (1999) 943.
[13] R. Mittal, P. Moin, Suitability of upwind-biased finite difference schemes for large-eddy simulation of turbulent flows, AIAA J. 35 (8) (1997) 1415.
[14] Y. Morinishi, T.S. Lund, O.V. Vasilyev, P. Moin, Fully conservative higher order finite difference schemes for incompressible flow, J. Comput. Phys. 143 (1998) 90.
[15] Y. Morinishi, O.V. Vasilyev, T. Ogi, Fully conservative finite difference scheme in cylindrical coordinates for incompressible flow simulations, J. Comput. Phys. 197 (2004) 686.
[16] M. Peric, A finite volume method for the prediction of three-dimensional fluid flow in complex ducts, Ph.D. Dissertation, University of London, 1985.
[17] M. Peric, R. Kessler, G. Scheuerer, Comparison of finite-volume numerical methods with staggered and collocated grids, Comput. Fluids 16 (1988) 389.
[18] C.M. Rhie, W.L. Chow, A numerical study of the turbulent flow past an isolated airfoil with trailing edge separation, AIAA J. 21 (1983) 1525.
[19] W. Rodi, S. Majumdar, B. Schonung, Finite volume methods for two-dimensional incompressible flows with complex boundaries, Comput. Methods Appl. Mech. Engrg. 75 (1989) 369.
[20] R.S. Rogallo, Numerical experiments in homogeneous turbulence, NASA Tech. Memo. 81315 (1981).
[21] M. Rosenfeld, D. Kwak, M. Vinokur, A fractional step solution method for unsteady incompressible Navier–Stokes equations in generalized coordinate systems, J. Comput. Phys. 94 (1991) 102.

[22] W. Shyy, T.C. Vu, On the adoption of velocity variable and grid system for fluid flow computation in curvilinear coordinates, J. Comput. Phys. 92 (1991) 82.
[23] Tannehill, Anderson, Pletcher, Computational fluid mechanics and heat transfer, second ed., Taylor and Francis, 1997.
[24] J. van Kan, A second-order accurate pressure correction method for viscous incompressible flow, SIAM J. Sci. Statist. Comput. 7 (1986) 870.
[25] O.V. Vasilyev, High order finite difference schemes on non-uniform meshes with good conservation properties, J. Comput. Phys. 157 (2000) 746.
[26] A.E.P. Veldman, K. Rinzema, Playing with non-uniform grids, J. Engrg. Math. 26 (1992) 119.
[27] R.W.C.P. Verstappen, A.E.P. Veldman, Spectro-consistent discretization of Navier–Stokes: a challenge to RANS and LES, J. Engrg. Math. 34 (1998) 163.
[28] R.W.C.P. Verstappen, A.E.P. Veldman, Preserving symmetry in convection–diffusion schemes, in: D. Drikakis, B.J. Geurts (Eds.), Turbulent Flow Computation, Kluwer Academic Publishers, 2002, p. 75.
[29] P. Wesseling, A. Segal, J. van Kan, C.W. Oosterlee, C. Kassels, Finite volume discretization of the incompressible Navier–Stokes equations in general coordinates on staggered grids, Comput. Fluid Dyn. J. 1 (1992) 27.
[30] J. Ye, J.A. McCorquodale, R.M. Barron, A three-dimensional hydrodynamic model in curvilinear coordinates with collocated grid, Int. J. Numer. Methods Fluids 28 (1998) 1109.
[31] Y. Zang, R.L. Street, J.R. Koseff, A non-staggered grid, fractional step method for time-dependent incompressible Navier–Stokes equations in curvilinear coordinates, J. Comput. Phys. 114 (1994) 18.